JOURNAL OF APPLIED ELECTROCHEMISTRY 22 (1992) 1025–1030

Raney-nickel activated H_2-cathodes Part I: Modelling the current/voltage behaviour of flat Raney-nickel coated microporous electrodes

S. RAUSCH, H. WENDT

Institut für Chemische Technologie, TH-Darmstadt, Germany

Received 2 September 1991; revised 23 December 1991

The current voltage behaviour of hydrogen evolving electrodes covered with a closed, smooth layer of Raney-nickel has been treated theoretically. Since the pores of Raney-nickel typically are from 1 to 10 nm wide, they are able, according to the Young–Laplace equation, to keep evolved hydrogen in solution up to concentrations of the order of 0.1 mol dm^{-3} which correspond to very high effective pressures of the order of 100 MPa. High concentrations of dissolved hydrogen cause substantial concentration-polarisation in the pores even at pore depths of several tenths of micrometres. The consequence is a limited effective pore length and catalyst utilization, respectively. This results in current voltage curves with steadily increasing Tafel slopes, which reach a limiting value of 140 mV dec^{-1} ($\alpha = 0.5$) at 90° C at current densities well above 1000 mA cm^{-2}.

1. Introduction

Raney-nickel, originally developed as a hydrogenation catalyst in organosynthesis, was introduced as an electrocatalyst for anodic hydrogen oxidation in alkaline fuel cells in 1960 by Justi and Winsel [1]. Soon afterwards it was also tried as an electrocatalyst for cathodic hydrogen evolution from alkaline solution and proved to be very effective and stable [2]. Today two different industrial methods are practised for the application of Raney-nickel coatings on steel or nickel electrodes: (i) the cold rolling of a mixture of Raney-nickel precursor 50 wt % Ni/Al-alloy and Mond-nickel (carbonyl-nickel) on to steel or nickel plates (used as supporting electrode). This coating can further be fixed by nickel deposition from an ordinary nickel-plating bath [2, 3]; and (ii) the cathodic deposition of a Ni/Zn-precursor alloy [4, 5], containing more than 50 wt % of zinc.

Both types of coating are finally leached by caustic potash leaving a more or less homogeneous coating of Raney-nickel which covers the surface of the support. (For details, see [4]). The theory of Raney-nickel anodes for fuel cells, which are usually composed of either sintered or PTFE-bonded (for instance, see [6]) Raney-nickel grains of 3 to 20 μm diameter is well developed. According to Mund and Ewe [7, 8], the competition between hydrogen diffusion into the Raney-nickel grain and its oxidative consumption by charge transfer at the inner surface of these particles leads to depletion of hydrogen with increasing pore length and to only limited utilization of the inner Raney-nickel surface in larger catalyst particles. This phenomenon is comparable to the phenomenon of limited catalyst utilization in heterogeneous chemical catalysis where the adimensional "Thiele modulus" determines the degree of utilization of the catalyst [9].

For hydrogen evolving Raney-nickel coated cathodes a similar treatment has not yet been carried out. Since in these electrodes hydrogen has to diffuse from the deeper parts of the pore towards the pore mouth and since in the very narrow pores of Raney-nickel a high concentration of dissolved hydrogen, which corresponds to very high hydrogen pressure, are expected to be built up, it is not *a priori* clear whether Mund's treatment of Raney-nickel anodes can be applied to Raney-nickel coated cathodes. Figure 1 compares the current–voltage curves for hydrogen evolution at a non-activated nickel electrode and a nickel electrode which is covered by a 60 μm thick coating of Raney-nickel.

2. Structural features of Raney-nickel and Raney-nickel coatings

It is well known that Raney-nickel precursors like Ni/Al (50/50 wt %) or Ni/Zn (20/80 wt %) shrink upon leaching of the non noble component, aluminium or zinc, and that the Raney-catalyst proper has only about 20% porosity instead of the expected 70% to 80% porosity, which may be anticipated from the volume fraction of zinc in a 20/80 mol % alloy [4, 10]. The pores created by leaching are very narrow. Their diameters range from 1 to 10 nm with a mean value of 4 nm. The determination of the inner surface leads to typical values of 50 $m^2 g^{-1}$ [11]. The cathodic deposition of Ni/Zn-precursor alloys on nickel supports usually yields dense and smooth coatings, the surfaces of which sometimes exhibit a rough appearance but never dendritic deposits (*cf.* [10]). Electrodes covered by rolled mixtures of Raney-nickel precursor (Ni/Al 50/50 wt %) and Mond nickel have a smooth surface but the coatings exhibit a macroporous granular structure, since the hard precursor granules are

0021-891X/

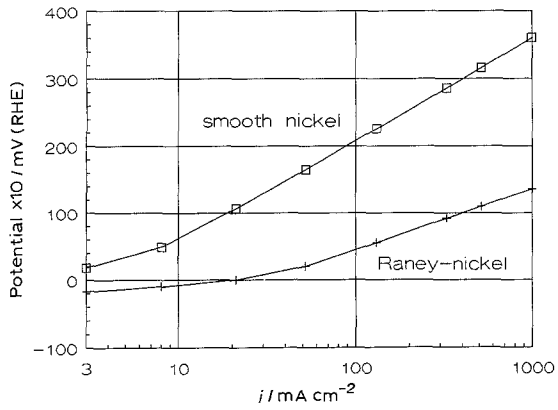

Fig. 1. Comparison of current–voltage curves of smooth and Raney-nickel coated nickel electrodes. Electrolyte 40 wt % KOH, 120° C, thickness of Raney-nickel coating 60 μm.

embedded in, and bound to, a coherent phase of relatively soft and ductile Mond nickel particles which has a sponge like morphology. Since leaching of these coatings causes shrinking of the precursor alloy, the morphology of both types of coatings changes in this process of catalyst formation. But this effect acts quite differently on the macroporosity of the two different coatings. The galvanically applied coating typically forms irregular, deep cracks which reach from the surface down to the supporting metal, whereas in the rolled coatings pores of micrometre thickness are forming a system of coarser voids penetrating the leached coating evenly. For a first simplified theoretical approach it is unnecessary to take account of the coarse porosity of these layers. Any refinements, for instance accounting for an additional coarse porosity in a rolled or sintered Raney-nickel cathode, may be performed in a second step for instance by introducing De Levy's [12] well known approach for porous electrodes.

3. Modelling of current voltage curves for Raney-nickel coated cathodes

In the present model, Raney-nickel coatings are assumed to be ideally flat and homogeneous. They possess homogeneous microporosity of approximately 20–40%. The pores are assumed to be of equal size with a pore radiuis, r, of the order of nanometres extending at right angles from the surface. These pores, with a surface to volume ratio of the order of $2/r = 10^7\,\mathrm{cm}^{-1}$ account for an interior surface of $4 \times 10^6\,\mathrm{cm}^2\,\mathrm{cm}^{-3}$ in a catalyst with 40% porosity which equals a mass specific inner surface of approximately $75\,\mathrm{m}^2\,\mathrm{g}^{-1}$, a value typically found for Raney-nickel. Infinite extension of the coatings and pores is assumed which, in practical terms, means that the coatings have a thickness of more than 100 μm. The modelling treats hydrogen production and diffusion in single pores and treats the porosity of the catalyst layer as a freely adjustable parameter. All pores are considered to be completely flooded by electrolyte Fig. 2. According to the Young–Laplace equation,

$$p_{bf} - p_s = (2\sigma\cos\theta)/r \qquad (1)$$

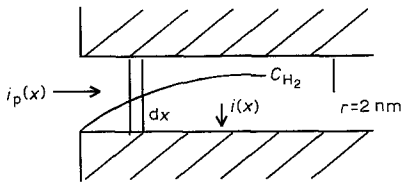

Fig. 2. Schematic representation of a single Raney-nickel pore with typical pore radius of 2 nm. The concentration of dissolved hydrogen increases with increasing pore depth.

where $p_s = 1$ bar and assuming complete wetting ($\cos\theta = 1$) the bubble formation pressure, p_{bf}, relative to $p_s = 1$ bar, is given by

$$p_{bf} = 2\sigma/r \qquad (2)$$

The surface tension, σ, of 30 wt % KOH against vapour saturated air at 90° C amounts to $7.8 \times 10^{-2}\,\mathrm{N\,m}^{-1}$ [13] so that with the assumed pore radius $r = 2 \times 10^{-7}$ cm the remarkably high bubble formation pressure of $p_{bf} = 80$ MPa is obtained. Figure 2 explains the pore model and these assumptions. Since hydrogen in 30 wt % KOH has a saturation concentration of approximately $10^{-4}\,\mathrm{mol\,dm}^{-3}$ under 1 bar hydrogen-pressure [14], this bubble formation pressure gives, by Raoult's law, an upper concentration limit of approximately $0.08\,\mathrm{mol\,dm}^{-3}$ of hydrogen under a pressure of 80 MPa. Even if the calculated hydrogen concentration in the pores exceeds the critical value of $0.08\,\mathrm{mol\,dm}^{-3}$ the pores will still be assumed to be flooded. This assumption is made because it is not certain whether Equation 1 is valid at almost molecular dimensions and, secondly, it is interesting to explore how far this concentration threshold is exceeded under practical current densities of the order of $1\,\mathrm{A\,cm}^{-2}$.

Because of the remarkably high hydrogen concentration levels in the micropores of the catalyst, appreciable diffusive mass transfer velocities of dissolved hydrogen across short distances can be visualized in the pores, matching the internal generation rates of hydrogen by cathodic decomposition of water:

$$H_2O + e^- = \tfrac{1}{2}H_2 + OH^- \qquad (3)$$

The surface specific rate $r_s(x)$ of Reaction 3 at distance x from the pore mouth ($x = 0$) is given by the local current density $i(x)$ at the pore wall (see Fig. 2):

$$r_s(x) = i(x)/2F \qquad (4)$$

which leads to the volume specific hydrogen evolution rate $r_v(x)$ within the pore:

$$r_v(x) = \frac{2\pi r\,\mathrm{d}x\,i(x)}{\pi r^2\,\mathrm{d}x\,2F} = \frac{i(x)}{rF} \qquad (5)$$

The balance of cathodic hydrogen generation and diffusion (Equation 6) at a distance x from the mouth of the pore (where c is the concentration of hydrogen molecules) reads

$$\left(\frac{\mathrm{d}c}{\mathrm{d}t}\right)_x = D\left(\frac{\mathrm{d}^2c}{\mathrm{d}x^2}\right)_x - r_v(x) \qquad (6)$$

and translates for steady state conditions into

$$\left(\frac{d^2c}{dx^2}\right)_x = \frac{i(x)}{rFD} \tag{7}$$

The local cathodic current density is given by the Butler–Volmer relation (Equation 8) and is determined by the actual local overpotential $\eta(x)$:

$$i(x) = i_0 [\exp(\alpha^+ F\eta(x)/RT) - \exp(-\alpha^- F\eta(x)/RT)] \tag{8}$$

The cathodic and anodic charge transfer coefficients, $\alpha^\pm$, for the hydrogen reaction are almost equal and set to 0.5 (*cf.* [15]). The exchange current density, i_0, is assumed to be independent of the hydrogen concentration as obtained for pressures up to 30 bar [16]. The local cathodic overpotential is obtained by subtracting from the overpotential at the pore mouth $\eta(x = 0)$ the local concentration overpotential $\eta_c(x)$ and ohmic voltage drop U_Ω:

$$\eta(x) = \eta(x = 0) - \eta_c(x) - U_\Omega \tag{9}$$

The concentration overpotential $\eta_c(x)$ is given by the hydrogen concentration $c(x)$ through the Nernst equation (Equation 10). The concentration of water and OH^- ions are assumed to be constant over the whole pore length because of their high concentrations in comparison to the relatively low hydrogen concentration of maximally $0.08\,mol\,dm^{-3}$ ($c_{H_2O} = 50\,mol\,dm^{-3}$ and $c_{OH^-} = 7\,mol\,dm^{-3}$) and diffusion coefficients for H_2O and OH^- which are of the same order of magnitude as for hydrogen.

$$\eta_c(x) = RT/2F \ln c(x)/c(0) \tag{10}$$

The quantity x extends from the surface of the coating ($x = 0$) down the pore axis. The ohmic voltage drop U_Ω is obtained by adding the electrolytic ohmic voltage drop to the ohmic voltage drop in the metallic matrix of the catalyst layer; the latter, however, is virtually zero since the specific conductivity of the nickel matrix ($\kappa_{Ni} = 1.35 \times 10^5\,\Omega^{-1}cm^{-1}$ [17]) is much higher than the electrolyte conductivity ($\kappa_{el} = 1\,\Omega^{-1}cm^{-1}$) [18]:

$$U_\Omega(x) = 1/\kappa_{el} \int_0^x i_p(x)\,dx \tag{11}$$

or written in differential form

$$\frac{dU_\Omega}{dx} = i_p(x)\,\kappa_{el} \tag{12}$$

The current density $i_p(x)$ in Equation 11 is the ionic current density in the pore, i.e. the local ionic current in the pore related to the pore cross section. The ionic current density in the pore $i_p(x)$ is obtained by integrating the increments of the wall surface related current density $i(x)$ at distance x from the pore mouth:

$$i_p(x) = \frac{2}{r} \int_\infty^x i(x)\,dx \tag{13}$$

Accordingly, the current density measured at the pore mouth $i_p(0)$, that means the current density referred to the cross section of the pore with which the pore generates hydrogen is given by:

$$i_p(x = 0) = \frac{2}{r} \int_\infty^0 i(x)\,dx \tag{14}$$

This effective pore current density defines the gradient of the hydrogen concentration at the pore mouth since the current density, $i_p(x)$ at point x defines the concentration gradient at this point:

$$\left(\frac{dc}{dx}\right)_x = \frac{i_p(x)}{2DF} = \frac{1}{DFr} \int_\infty^x i(x)\,dx \tag{15}$$

Substituting the pore current density $i_p(x)$ from Equation 12 into Equation 15 and integration leads to an expression for the ohmic drop in the pore in terms of the hydrogen concentration $c(x)$:

$$U_\Omega(x) = \frac{2FD}{\kappa_{el}} (c(x) - c(0)) \tag{16}$$

the combination of Equations 7 to 10 and 16 yields the differential (Equation 17) which has to be solved numerically. That is,

$$\begin{aligned}\left(\frac{d^2c}{dx^2}\right)_x = \frac{i_0}{rFD} \Bigg[& \exp\left(\frac{0.5F\eta(0)}{RT}\right) \left(\frac{c(0)}{c(x)}\right)^{0.25} \\ & \times \exp\left(-\frac{F^2D}{RT\kappa_{el}}\right)(c(x) - c(0)) \\ & - \exp\left(-\frac{0.5F\eta(0)}{RT}\right) \left(\frac{c(x)}{c(0)}\right)^{0.25} \\ & \times \exp\left(\frac{F^2D}{RT\kappa_{el}}\right)(c(x) - c(0))\Bigg]\end{aligned} \tag{17}$$

Boundary conditions for a pore of infinite extension are

$$c(x = 0) = c_s\,(1\,bar\ hydrogen) \tag{18}$$

$$(dc/dx)_{x=0} = i_p(0)/2DF \tag{19}$$

$$(dc/dx)_{x=\infty} = \eta_{H_2}(\infty) = i(\infty) = i_p(\infty) = \eta(\infty) = 0 \tag{20}$$

The boundary condition of Equation 20 is identical to the condition that the sum of hydrogen concentration polarization overvoltage and ohmic drop at infinite distance from the pore mouth equals the externally applied overpotential which means that at long distances from the pore mouth the pore wall no longer produces hydrogen.

4. Mathematical methods and parameter choice

The issue is to correlate total pore current densities with externally applied overpotential $\eta(0)$. Since the Butler–Volmer equation at overpotentials of more than 60 mV becomes nonlinear in overpotential, η, and since the concentration overpotential Equation 11 is logarithmic in the local concentration of hydrogen, the differential equation (17) cannot be solved in closed form. Instead it is solved numerically by the procedure of Euler–Cauchy by successive iteration transforming the differential Equation (17) into a difference equation combined with a shooting method.

First, an overvoltage $\eta(0)$ and a pore current density $i_p(0)$ are given, from which the hydrogen concentration gradient $(dc/dx)_{x=0}$ at the pore mouth $x = 0$ is calculated according to Equation 15. Starting at the hydrogen saturation concentration $c(0)$ at $x = 0$ the concentration $c(x + dx)$ at the point $x + dx$ is calculated by the following:

$$c(x + dx) = c(x) + (dc/dx)_x \Delta x \quad (21)$$

$$(dc/dx)_{x+dx} = (dc/dx)_x + (d^2c/dx^2)_{x+dx} \Delta x \quad (22)$$

With Equations 8–10, 15, and Equations 17 and 22, the quantities $(d^2c/dx^2)_{x+dx}$ and $(dc/dx)_{x+dx}$ at the point $x + dx$ can be calculated. Repeating this procedure the whole hydrogen concentration profile $c(x)$ can be calculated until the concentration gradient dc/dx becomes zero. Then it is checked whether the overvoltage $\eta(\infty) = 0$ or $\eta_c(\infty) = \eta(0)$ (boundary condition Equation 20). If this does not apply the starting value $\eta(0)$ is changed and a new profile is calculated.

The pores are completely filled with electrolyte and the high conductivity of 30% KOH at 90° C of $\kappa_{el} = 1.3\,\Omega^{-1}\,cm^{-1}$ gives negligible ohmic drops. At typical pore current densities $i_p(0)$ of $1\,A\,cm^{-2}$ and a maximal pore length of 100 μm, U_Ω is in the range of a few millivolts. Therefore neglecting the ohmic drop in the pore equation (9) simplifies to

$$\eta(x) = \eta(x = 0) - RT/2F \ln c(x)/c(0) \quad (23)$$

$$\left(\frac{d^2c}{dx^2}\right)_x = \frac{i_0}{rFD}\left[\exp\left(\frac{0.5F\eta(0)}{RT}\right)\left(\frac{c(0)}{c(x)}\right)^{0.25} - \exp\left(-\frac{0.5F\eta(0)}{RT}\right)\left(\frac{c(x)}{c(0)}\right)^{0.25}\right] \quad (24)$$

From Equation 23 the maximum hydrogen concentration at infinite distance from the pore mouth $c(\infty)$ can be calculated for a given externally applied overpotential $\eta(0)$:

$$c(\infty) = c(0) \exp(RT\eta(0)/2F) \quad (25)$$

Standard conditions for alkaline water electrolysis are 30% KOH solution and 90° C. The hydrogen saturation concentration $c(0)$ under these conditions at 1 bar amounts to $8 \times 10^{-5}\,mol\,dm^{-3}$, the hydrogen diffusion coefficient to $7 \times 10^{-5}\,cm^2\,s^{-1}$ [20] and the electrolytic conductivity κ_{el} to $1.3\,\Omega^{-1}\,cm^{-1}$. These parameters were kept constant for all calculations.

The solution of the differential expression in Equation 24 for a given applied overpotential $\eta(0)$ and the prefactor i_0/rFD yields a concentration profile $c(x)$ from which the pore current density $i_p(0)$ can be calculated as well as the concentration gradient at the pore mouth. As parameters the externally applied overvoltage $\eta(0)$ and the exchange current density i_0, which determine the prefactor in Equation 24, were varied. The pore radius r was chosen as 2 nm and was held constant for all calculations.

5. Results and discussion

In Fig. 3 the hydrogen concentration profile $c(x)$ for a pore current density $i_p(0)$ of $400\,mA\,cm^{-2}$ and the overvoltage distribution with an overvoltage at the pore mouth of $\eta(0) = 78$ mV are shown. These profiles are calculated for an exchange current density $i_0 = 10^{-4}\,A\,cm^{-2}$ which is reported for smooth nickel in 30% KOH at 90° C [19]. Because the overvoltage $\eta(x)$ falls sharply close to the pore mouth, the current penetration depth, defined arbitrarily by the pore length at which the pore current density $i_p(x)$ is decreased to 1/e of the pore current density $i_p(0)$ at the pore mouth, is only 4 μm. The hydrogen concentration far away from the pore mouth $c(\infty) = 0.011\,mol\,dm^{-3}$ (137 bar) produces a concentration overvoltage of 78 mV which equals the applied overvoltage $\eta(0)$, Equation 25.

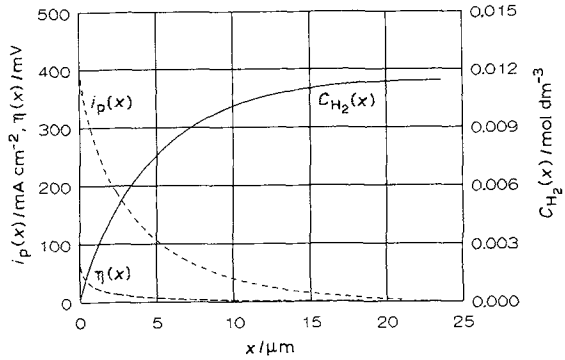

Fig. 3. Calculated dissolved hydrogen profiles of c_{H_2}, pore current density, i_p, and cathodic overpotential, $\eta(x)$, against depth of a single pore. $r = 2$ nm, $i_0 = 10^{-4}\,A\,cm^{-2}$, externally applied overpotential $\eta(0) = -78$ mV.

In Fig. 4 the pore current density $i_p(0)$ and the hydrogen concentration gradient at the pore mouth $(dc/dx)_{x=0}$ are doubled. Thereupon the hydrogen concentration $c(\infty)$ in the depth of the pore and the externally applied overvoltage increase to $0.047\,mol\,dm^{-3}$ (587 bar) and to 100 mV, respectively. Most important to note is that the current penetration depth does not decrease but increases with increasing current density from 4 to 7 μm.

The influence of i_0 for an overvoltage $\eta(0)$ of 78 mV is depicted in Fig. 5, which is calculated for i_0-values of 10^{-3} and $10^{-4}\,A\,cm^{-2}$. By increasing i_0, by a factor of 10, the hydrogen concentration gradient at the pore mouth (Equation 15) and the pore current density

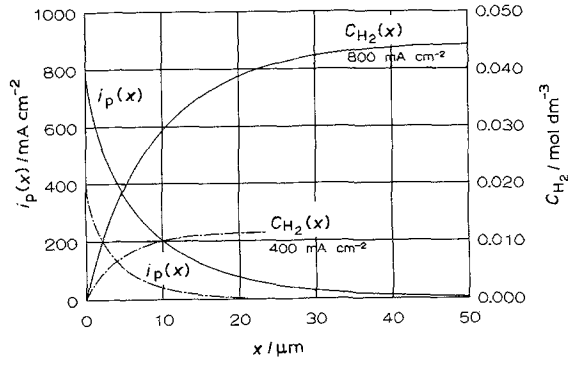

Fig. 4. Profiles of hydrogen concentration and pore current densities $i_p(0)$ in Raney-nickel pores at 400 and 800 mA cm^{-2} at the pore mouth; $r = 2$ nm; $i_0 = 10^{-4}\,A\,cm^{-2}$, overpotentials amount to -78 and -100 mV, respectively.

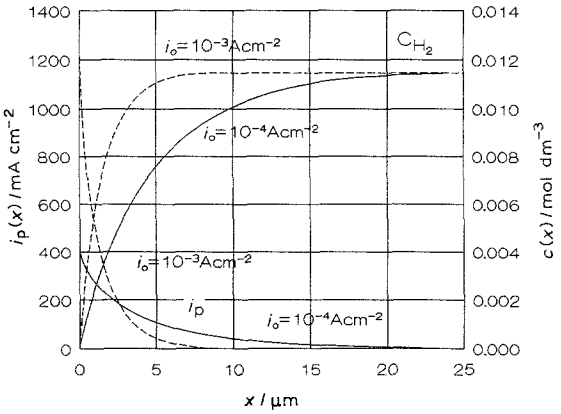

Fig. 5. Profiles of hydrogen concentration and pore current density for two different exchange current densities $i_0 = 10^{-3}$ and 10^{-4} A cm^{-2} and equal overpotential $\eta(0) = -78$ mV. The pore current densities are $i_p(0) = 1200$ and 400 mA cm^{-2}.

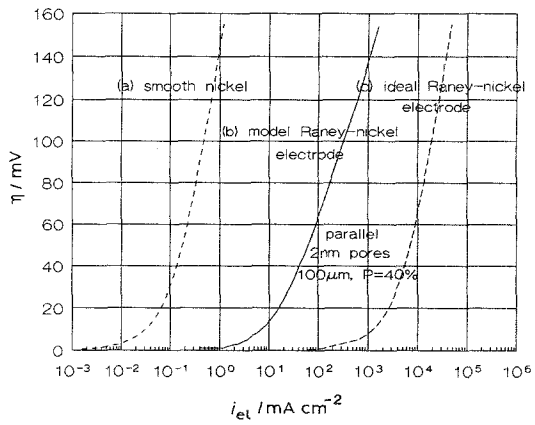

Fig. 7. Comparison of calculated current voltage curves (a) smooth nickel electrode, (b) Raney-nickel electrode with limited utilization, (c) Raney-nickel electrode with hypothetical full utilization.

$i_p(0)$ increase by a factor of approximately 3 from 400 to 1260 mA cm^{-2}. Simultaneously the current penetration depth decreases by a factor of four from 4 to 1 μm.

In Fig. 6 the calculated penetration depth of the pore current density is calculated as function of the pore current density $i_p(0)$ for three different exchange current densities i_0 (10^{-3}, 10^{-4}, 10^{-5} A cm^{-2}) for a 2 nm pore. The penetration depth increases with decreasing exchange current density i_0 and decreasing pore current density $i_p(0)$.

In Fig. 7 three differently calculated hydrogen-evolving cathodes are compared. For all three calculations the identical exchange current density $i_0 = 10^{-4}$ A cm^{-2} was used. The three different electrodes are a smooth nickel electrode, a Raney-nickel coated electrode with homogenous coating and hydrogen overpotential due to slow diffusive mass transfer (model Raney-nickel electrode), a Raney-nickel coated electrode whose coating is assumed to be fully utilized without hydrogen accumulation and without assso-ciated concentration overpotential (ideal Raney-nickel electrode). The Raney-nickel electrodes consist of parallel 2 nm pores and have a porosity P of 40% which is equal to a weight specific inner surface of 75 m^2 g^{-1} and a surface specific inner surface of 4 m^2 cm^{-2} at an assumed coating thickness of 100 μm.

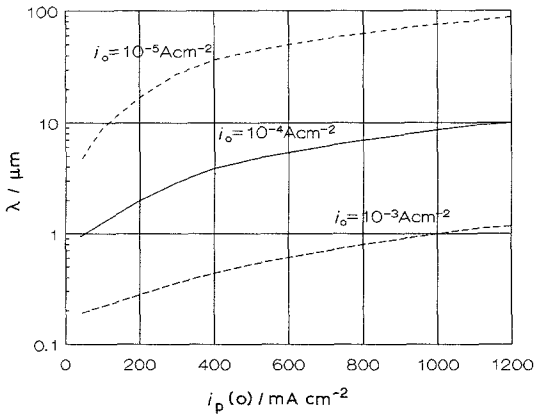

Fig. 6. Dependence of penetration depth on pore current density with exchange current density as parameter.

The effective current density of the electrode, i_{el}, is calculated from the pore current density $i_p(0)$ overvoltage behaviour of a 2 nm pore accounting for the porosity, P:

$$i_{el} = i_p(0)P \tag{26}$$

At a current density of 1 A cm^{-2} the cathodic overvoltage for the Raney-nickel cathode with concentration polarisation is 100 mV which is typical of Raney-nickel electrodes. This current density overvoltage correlation is compared with the theoretical curves calculated from the Butler–Volmer equation (8) for smooth nickel electrodes and the same Raney-nickel coated electrode assuming unrestricted full utilization of the inner surface of the Raney-nickel coating. The Tafel slope of the smooth and the ideal Raney-nickel coated electrode above 1 and 10^4 mA cm^{-2}, respectively, is 140 mV dec^{-1} whereas the slope of the calculated model electrode is only 80 mV dec^{-1} at a current density between 100 mA cm^{-2} and 1 A cm^{-2}. Figure 6 shows that the penetration depth of the pore current is always lower than 10 μm ($i_0 = 10^{-4}$ A cm^{-2}) and increases with increasing pore current density. This means that the degree of utilization of 100 μm thick model Raney-nickel coating is always lower than 10% and that the utilized inner surface of the electrode is a function of the current density. In contrast to fuel cell anodes the utilization of hydrogen-evolving Raney nickel coatings improves with increasing current density.

The Tafel slope of the model electrode increases continuously with increasing current density reaching a limiting value of 140 mV dec^{-1} though at very high current densities at a catalyst utilization of 100% (Fig. 7). This model calculation predicts Tafel slopes of 80–110 mV dec^{-1} at intermediate current densities which are actually observed with galvanically deposited Raney-nickel cathodes with a coating thickness of up to 150 μm (see Fig. 1).

It is important to distinguish the described micropore model from the macropore models of de Levy [12] and Winsel [1]. In macroporous (d_p = 1–10 μm) electrodes of a thickness of up to 1000 μm the ohmic drop in the macropores (1–10 μm) is substantial. In

such macroporous electrodes the current penetration depth decreases with increasing current density due to the ohmic drop in the macropores. The result is a Tafel slope higher than 140 mV dec^{-1} which is predicted to be double that for smooth electrodes. Raney-nickel coatings prepared by sintering or cold rolling of Raney-nickel precursor alloy with carbonyl nickel have a thickness of up to 500 μm. In such electrodes the degree of utilization of a single Raney-nickel grain ($< 50\,\mu$m) is described by the given microporous (1–5 nm) model whereas the utilization of the whole layer should be calculated by a macroporous (1–5 μm) model which accounts for the ohmic drop in the macropores.

6. Conclusion

The model calculations treating idealized, single micropores (1–10 nm) of a catalytic Raney-nickel coating of a hydrogen evolving cathode which are completely filled with electrolyte with hydrogen concentrations corresponding to pressures of up to 800 bar show that the current penetration depth in such pores is in the range of only a few micrometres. The reason is that the diffusive transport of the dissolved hydrogen is relatively slow so that due to high concentration polarization the internal surface of the pore becomes electrochemically inactive. Therefore the degree of catalyst utilization in such idealized Raney-nickel layers is predicted to be relatively low. Raney-nickel coatings of hydrogen evolving cathodes should therefore not form a closed homogeneous layer. Instead such layers should be subdivided by coarse pores and cracks.

Further the calculations show that the current penetration depth increases with increasing current density, which is in contrast to macroporous models which only take account of the ohmic drop in the pore. Raney-nickel cathodes with a coating thickness of up to 150 μm have an abnormal Tafel slope of only 80–110 mV dec^{-1} in the current density range 0.1 to 1 A cm^{-2} which can be now easily explained by the fact that the useful, inner electrode surface increases with increasing current density.

References

[1] E. Justi, M. Pilkuhn, W. Scheibe and A. Winsel, Akad. Wissenschaften und Literatur, Braunschweig, Abhandlg. Mathem. Naturw, Klasse **8** (1959); E. Justi and A. Winsel, 'Kalte Verbrennung-Fuel Cells', Franz Steiner Verlag GmbH, (1962).
[2] K. Lohrberg and P. Kohl, *Electrochim. Acta* **29** (1984) 1557.
[3] J. Divisek and H. Schmitz, German patent application P 3 743 354.7.
[4] V. Plzak and H. Wendt, *Chem. Ing. Tech.* **58** (1986) 415.
[5] J. Divisek, H. Schmitz and H. Wüllenweber German patent DE 3 330 961.
[6] H. Sauer, German patent DE-OS 2 941 774 (1979).
[7] K. Mund, *Siemens Forsch. u. Entwickl. Berichte* **4** (1975) 68.
[8] H. Ewe, 'Habilitation', Braunschweig (1974).
[9] J. M. Coulson and J. F. Richardson, 'Chemical Engineering', Vols 1–4, Pergamon Press, Oxford (1980).
[10] Electrochemical Hydrogen Technologies (edited by H. Wendt), Elsevier, Barking GB (1990).
[11] P. Brennecke and H. Ewe, *Chem.-Ing.-Tech.* **52** (1980) 426.
[12] 'Advances in Electrochemistry and Electrochemical Engineering', Vol. 6 (edited by R. de Levy and P. Delahay), Interscience Publishers, Wiley & Sons, New York (1967) p. 329.
[13] K. Feldkamp, *Chem.-Ing.-Tech.* **41** (1969) 21.
[14] F. Knaster and A. Apelbaum, *Russ. J. Phys. Chem.* **1** (1964).
[15] K.J. Vetter, 'Elektrochemische Kinetik', Springer, Berlin (1961).
[16] H. Cassel and E. Krumbein, *Z. Physik. Chem.* **A171** (1934) 70.
[17] 'Handbook of Chemistry and Physics', CRC Press, Boca Raton (1986).
[18] L. Yushkevich, *Electrokhimiya* **3** (1967) 1481.
[19] G. Kreysa and B. Hankansson, *J. Electroanal. Chem.* **201** (1986) 61.
[20] C. Tham, F. Walker and B. Gubbins, *J. Phys. Chem.* **74** (1970).